

Visualization of the Energy-Containing Turbulent Scales

Anders Helgeland*
UniK

Øyvind Andreassen†
FFI

Atle Ommundsen
FFI
Trond Gaarder
FFI

B. Anders Pettersson Reif
FFI

Joe Werne‡
CoRA/NWRA

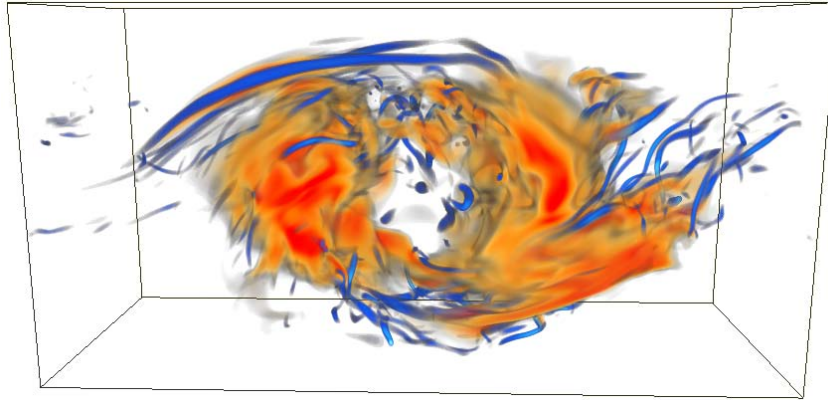


Figure 1: Two-field visualization of a Kelvin-Helmholtz billow at time $t = 105 h/U_0$ in the simulation. The orange field shows the kinetic energy (large-scale turbulence features) while the blue field reveals vortex structures rendered by the λ_2 criterion (small-scale turbulence features). Kelvin-Helmholtz billows occur fairly frequently in the atmosphere, with wavelength up to a few kilometers. As they induce vertical air motion, they sometimes generate billow clouds.

ABSTRACT

In this study, we explore a novel approach for visualizing the energetic turbulent structures in a flow field. The flow field is generated by a direct numerical simulation (DNS) of a stratified turbulent shear layer instigated by the Kelvin-Helmholtz instability. The use of so-called structure-based tensors combined with volume rendering seems to be a very promising tool to gain new insight into the dynamically most important part of the turbulence. Rendering of these tensors depicts the large-scale structures that carry most of the turbulence energy. This is in distinct contrast to traditional methods based on derivatives of the velocity field, such as those based on the velocity gradient tensor and vorticity. These methods only capture the smaller-scale structures of the flow. Traditionally, statistical measures are used to handle the enormous amount of data generated by DNS, whereby a lot of detailed information is inevitably lost. The rapid increase in computer performance combined with advanced visualization techniques makes it possible to use a non-statistical or deterministic approach to study the kinematic and dynamic properties of turbulent flows. This paper presents a promising first attempt to render structure-based tensors to see how faithfully they can describe the large-scale structures in a stratified turbulent shear flow.

*University Graduate Center (UniK), NO-2027 Kjeller, Norway. e-mail: ahe@ffi.no

†Norwegian Defence Research Establishment (FFI) NO-2027 Kjeller, Norway.

‡NorthWest Research Associates, CoRA Division, Boulder, CO 80301, USA.

CR Categories:

I.3.8 [Computer Graphics]: Applications— [I.4.7]: Image processing and Computer Vision—Feature representation I.4.10 [Image processing and Computer Vision]: Volumetric— [J.2]: Physical science and Engineering—Physics

Keywords: Features in volume data sets, Volume rendering of extremely large datasets, 3D Vector field visualization, Multi-field Visualization, Fluid Dynamics, Turbulence, Structure Tensors

1 INTRODUCTION

The rapid increase in computer performance over the last twenty years or so has made direct numerical simulations (DNS) of the three-dimensional and time dependent Navier-Stokes equations feasible. The enormous amount of data generated by DNS, however, is very difficult to handle and to analyze in an efficient manner. Traditionally, in order to overcome this problem, the data has been truncated by adopting a statistical approach. The amount of data is thereby effectively reduced – often from four to one dimension. Despite the loss of detailed information, invaluable understanding has nevertheless been obtained that has greatly impacted this research field. It is important to keep in mind, however, that statistical descriptions are motivated more by mathematical convenience than by physical attractiveness.

Advanced visualization algorithms and state-of-the-art computer architectures have recently provided means to face the turbulence problem in a new and different way. Instead of relying on statistical measures, a non-statistical or deterministic approach becomes feasible. This is possible because direct numerical simulations of turbulence contains *all* of the information needed to describe every detail of the flow field in both space and time. This sets the stage for a more complete picture of the kinematical and dynamical prop-

erties of turbulent flows, and this is why DNS has become such an invaluable tool for turbulence researchers. In order to assure a correct interpretation of the data, however, the physical processes of interest must be correctly represented by a mathematical model and properly visualized. Here lies one of the major challenges in data visualization of turbulent flow fields, and this is what motivates the present study.

The fluid dynamics of flows at high Reynolds numbers is characterized by the existence of several length-scales, some which assume very specific roles in the description and analysis of flows [20]. Turbulence, which truly is a *multi-scale* phenomena, can be thought of as a continuous hierarchy of eddies ranging from large to small scales, where the smaller eddies "feed" on the larger ones until the energy eventually passes into heat through viscosity at the smallest scales of motion¹. Even though this metaphor has been found to give a good quantitative picture of energy dynamics in turbulence, the precise nature of the turbulence structures (eddies) remains unclear.

The identification of turbulence structures has traditionally been based on identifying regions of the flow where the vorticity concentration is sufficiently high for a local roll up of the surrounding fluid to occur. The objective has thus been to identify "well-defined" coherent structures, such as vortices, within the flow field. Many vortex-detection methods have been proposed in the literature. Among the most popular and successful identifiers are enstrophy $||\omega^2||$ used by e.g. [4], the Q criterion [10], and the λ_2 [12], Predictor-Corrector [1], Eigenvector [19], Parallel Vectors [17], and Combinatorial [13] methods. Common to all of these methods is the direct use of velocity derivatives, such as the velocity gradient tensor and vorticity. For multi-scale physical processes like turbulence, this implies that the focus is on features closer to the *small-scales* of the flow field, i.e. the portion of the flow field where the turbulence energy is dissipated into heat by the action of viscosity. Although there is a coupling between small and large scales, the small-scale coherent structures do not in general reveal details about the morphology of the dynamically more important *large-scale* features. It is the large scales that carry most of the turbulence energy; it is in this portion of the flow where turbulence energy is produced. The objective of the present study is to apply a novel single-point methodology to characterize these energy-containing scales using volume visualization.

2 MATHEMATICAL PRELIMINARIES

The instantaneous velocity field $\mathbf{u}(\mathbf{x}, t)$ can without loss of generality be decomposed into mean and fluctuating parts, i.e.

$$u_i(\mathbf{x}, t) = U_i(\mathbf{x}, t) + u'_i(\mathbf{x}, t) \quad (1)$$

where $U_i = \langle u_i(\mathbf{x}, t) \rangle$ is the ensemble averaged mean velocity in the x_i direction, and u'_i denotes the fluctuating velocity component. The components of the instantaneous second-rank single-point (Reynolds-stress) tensor $R'_{ij}(\mathbf{x}, t) = u'_i u'_j$ is a product of two velocity components, and as such a measure of the kinetic energy, and it describes the *componentality* of the turbulence field, i.e. the strengths of different fluctuating velocity components. This is the traditional quantity used to characterize the energetic large-scale portion of the flow field. Its relation to the kinetic energy of the flow field becomes clear if we consider the special case of homogeneous turbulence. The turbulence is homogeneous if any correlation, e.g. $\langle u'_i u'_j \rangle$, is independent of spatial position. This enables us to express the fluctuating velocity in terms of a Fourier series expansion;

$$u'_i(\mathbf{x}) = \sum_{\mathbf{k}} \hat{u}'_i(\mathbf{k}) e^{-i\mathbf{k} \cdot \mathbf{x}} \quad (2)$$

¹The ratio of these scales, ranging from large scale L to small scale (dissipation) l_d , is related to the Reynolds number, Re , by $L/l_d = O(Re^{3/4})$.

and it thus follows that

$$R'_{ij} = \int E'_{ij}(\mathbf{k}) d^3 \mathbf{k}. \quad (3)$$

where the accent $\hat{\cdot}$ denotes a Fourier coefficient, \mathbf{k} is the wave-number vector and $E'_{ij} \equiv \hat{u}'_i(\hat{u}'_j)^*$ is the velocity spectrum tensor. The superscript $*$ denotes the complex conjugate. The components of R'_{ij} are thus related to the partition of energy in different directions in spectral space. It should be noted that the trace $R'_{kk} = R'_{11} + R'_{22} + R'_{33}$ is (twice) the turbulent kinetic energy.

2.1 Structure-based tensors

The Reynolds-stress tensor \mathbf{R}' alone is, however, not sufficient to completely quantify the state of turbulence because structural information characterizing flow morphology is absent. Kassinos et al. [14] point out that a complete one-point description may be possible by using so-called structure-based tensors. These are second- and third-rank tensors derived from correlations of gradients of the turbulence vector stream-function Ψ'_i defined as

$$\nabla^2 \Psi'_i = -\omega'_i, \quad (4)$$

where $\omega'_i = \varepsilon_{ijk} \partial_j u'_k$ is the fluctuating vorticity in the x_i direction. The fluctuating velocity components are related to the vector stream-function through the relation

$$u'_i = \varepsilon_{ijk} \partial_j \Psi'_k. \quad (5)$$

The conservation of mass requires $\partial_k u'_k = 0 \leftrightarrow \partial_k \Psi'_k = 0$. Here, ε_{ijk} is the Levi-Civita alternating tensor.

Kassinos et al. [14] then used the fluctuating vector stream-function Ψ'_i to form a set of second-rank single-point structure-based tensors:

$$D'_{ij} \equiv \partial_i \Psi'_k \partial_j \Psi'_k \quad \textit{Dimensionality} \quad (6)$$

$$F'_{ij} \equiv \partial_k \Psi'_i \partial_k \Psi'_j \quad \textit{Circulicity} \quad (7)$$

$$C'_{ij} \equiv \partial_k \Psi'_i \partial_j \Psi'_k \quad \textit{Inhomogeneity} \quad (8)$$

These tensors characterize the large-scale turbulence field. Together with R'_{ij} they form a minimal tensorial base for a complete single-point turbulence theory. Members of the subset R'_{ij} , D'_{ij} , F'_{ij} , and C'_{ij} are linearly independent and can be related to the trace of R'_{ij} through the following constitutive relation:

$$R'_{ij} + D'_{ij} + F'_{ij} - (C'_{ij} + C'_{ji}) = R'_{kk} \delta_{ij}. \quad (9)$$

The physical interpretation of these tensors is most conveniently evaluated in spectral space. Assuming homogeneity for convenience enables us to write

$$\Psi'_i(\mathbf{x}) = \sum_{\mathbf{k}} \hat{\Psi}'_i(\mathbf{k}) e^{-i\mathbf{k} \cdot \mathbf{x}} \quad (10)$$

$$\omega'_i(\mathbf{x}) = \sum_{\mathbf{k}} \hat{\omega}'_i(\mathbf{k}) e^{-i\mathbf{k} \cdot \mathbf{x}}. \quad (11)$$

In order to express the structure-based tensors in spectral space we start with the definition $\nabla^2 \Psi'_i = -\omega'_i$ which is equivalent to

$$\hat{\omega}'_i(\mathbf{k}) = k^2 \hat{\Psi}'_i(\mathbf{k}), \quad (12)$$

such that

$$\partial_j \Psi'_i(\mathbf{x}) = \sum_{\mathbf{k}} (-ik_j) \hat{\Psi}'_i(\mathbf{k}) e^{-i\mathbf{k} \cdot \mathbf{x}} = -\varepsilon_{ils} \sum_{\mathbf{k}} \frac{k_l k_j}{k^2} \hat{u}'_i(\mathbf{k}) e^{-i\mathbf{k} \cdot \mathbf{x}}. \quad (13)$$

2.1.1 The dimensionality tensor \mathbf{D}'

Substituting (13) into the definition (6) gives

$$D'_{ij} \equiv \partial_i \Psi'_k \partial_j \Psi'_k = \int \frac{k_i k_j}{k^2} E'_{mn} d^3 \mathbf{k}. \quad (14)$$

The dimensionality tensor \mathbf{D}' thus describes the anisotropy of length scales in physical space, i.e., it contains information that is distinct from that in R'_{ij} ; if, e.g. $D'_{11} = 0$, then $k_1 = 0$ and the large-scale turbulence field is independent of the spatial direction x_1 .

It should be noted that the trace of the dimensionality tensor is related to the turbulent kinetic energy: $D'_{kk} = R'_{kk} + C'_{kk}$.

2.1.2 The circulicity tensor \mathbf{F}'

The circulicity tensor \mathbf{F}' describes the large-scale vorticity field. This becomes clear by rewriting it in the following form

$$\begin{aligned} F'_{ij} &= \int k^2 \hat{\Psi}'_i (\hat{\Psi}'_j)^* d^3 \mathbf{k} = \int \mathcal{F}'_{ij}(\mathbf{k}) d^3 \mathbf{k} \\ &= \int k^{-2} \hat{\omega}'_i (\hat{\omega}'_j)^* d^3 \mathbf{k} = \int k^{-2} W'_{ij}(\mathbf{k}) d^3 \mathbf{k}, \end{aligned} \quad (15)$$

which shows that the circulicity spectrum tensor $\mathcal{F}'_{ij}(\mathbf{k})$ is related to the vorticity spectrum tensor $W'_{ij}(\mathbf{k})$ through the relation

$$\mathcal{F}'_{ij}(\mathbf{k}) = k^{-2} W'_{ij}(\mathbf{k}). \quad (16)$$

This directly implies a scale separation between circulicity and vorticity; the former is a measure of 'large-scale' (low wave-numbers) vorticity whereas the latter is a measure of 'small-scale' (high wave-numbers) vorticity. Similar scale separations exists between the circulicity tensor and any quantity containing derivatives of the velocity, such as the velocity gradient tensor. This is due to the fact that differentiation in physical space is equivalent to multiplication by the wave-number k in Fourier space. Methods that directly uses velocity derivatives will therefore, just like vorticity derived quantities, only detect the less energetic and smaller-scale turbulence structures. It should be mentioned that scale separations between small and large scale features only exist for multi-scale physical processes, such as turbulence (see section 1). This means that the vortex-detection methods based on velocity derivatives only will fail to detect the largest features when applied to multi-scale simulations. For single-scale simulations, all features like vortices are of "the same" length-scale and rendering of these structures are well depicted through traditional methods such as λ_2 .

If one of the diagonal components (in principal axes) of F'_{ij} dominates the others, then the largest turbulence scales engender rotation predominantly about that direction. It is important to note that \mathbf{F}' does *not* represent a vortex in general; it is related to the local variation of the vector stream-function and it does not require the 'structure' to be geometrically closed.

Similar to \mathbf{D}' , the trace of the circulicity tensor also relates to the turbulent kinetic energy: $F'_{kk} = R'_{kk} + C'_{kk}$.

2.1.3 The inhomogeneity tensor \mathbf{C}'

As the name already alludes to, the inhomogeneity tensor is a measure of the departure from homogeneity. By invoking mass conservation, (8) can be written as

$$C'_{ij} \equiv \partial_k \Psi'_i \partial_j \Psi'_k = \partial_k (\Psi'_i \partial_j \Psi'_k), \quad (17)$$

and it thus becomes clear that it is identically zero for homogeneous turbulence, i.e. $\langle C'_{ij} \rangle \equiv 0$.

2.2 Physical interpretation

The distinctive features of small-scale turbulence visualized based on the λ_2 criterion [12] for instance fulfill the definition of coherent vortices put forward by e.g. [15] and thus represent coherent *structures*. The large-scale morphology described by the structure-based tensors is very different in character. The information carried by the individual tensors is not independent, but it is the combination of all these individual contributions that gives the entire picture.

The interpretation is carried out point-wise in principal axes. In the new local coordinate system defined by the tensors' principal axes, the off-diagonal components of the dimensionality (\tilde{D}'_{ij}), circulicity (\tilde{F}'_{ij}) and componentality (\tilde{R}'_{ij}) tensors are all zero. These tensors are furthermore normalized $d_{ij} (\equiv \tilde{D}'_{ij} / \tilde{D}'_{kk})$, $f_{ij} (\equiv \tilde{F}'_{ij} / \tilde{F}'_{kk})$ and $r_{ij} (\equiv \tilde{R}'_{ij} / \tilde{R}'_{kk})$ such that $d_{ii} = 1$, $f_{ii} = 1$ and $r_{ii} = 1$.

The kinematical character of the structures is described by the two tensors \mathbf{r} and \mathbf{f} , which carries information about *jetal* and *curved* motion respectively. The spatial coherence is described by \mathbf{d} . Figure 2 displays a simple example of how the structure-based tensors are interpreted.

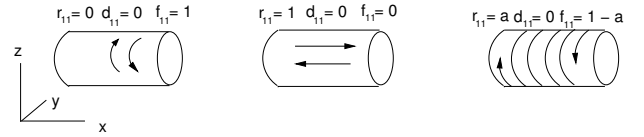


Figure 2: Schematic of large-scale structures.

2.3 Simple examples

To get a picture of what the structure tensors show us, let us consider two simple cases: (i) solid body rotation and (ii) plane shear flows. For case (i) the velocity components in cylindrical coordinates are given by $v_r = 0$, $v_\theta = \Omega r$, $v_z = 0$, where the angular velocity Ω is constant. The vorticity is $\omega_r = 0$, $\omega_\theta = 0$, $\omega_z = 2\Omega$. According to equations (4) or (5) the stream-function can be written $\Psi_r = 0$, $\Psi_\theta = 0$, $\Psi_z = -\Omega r^2/2$. The components of the dimensionality tensor become

$$D_{rr} = (\Omega r)^2, \quad D_{ij} = 0, \text{ for } i, j \neq r, \quad (18)$$

which shows that the velocity field only varies in the radial direction, which indeed is the case. The components of the circulicity tensor become

$$F_{zz} = (\Omega r)^2, \quad F_{ij} = 0, \text{ for } i, j \neq z, \quad (19)$$

which indicates a preferred circulicity about the axial (z) direction. As pointed out in Section 2.1.2, there is some similarity between circulicity and vorticity. While vorticity rendered through enstrophy will show vortex cores whose scales are close to the dissipative (small) scale, circulicity can be used to identify energy-containing vortical structures which are closer to the energetic (large) scale of turbulence. All components of the inhomogeneity tensor $C_{ij} = 0$.

For case (ii) we consider a planar shear flow $\partial_3 u_1 = A_0$, $u_2 = 0$, and $u_3 = 0$, where A_0 is a constant. No "vortex" is present in this case, but the vorticity has a planar distribution $\omega_2 = A_0$, of which a vortex sheet is a special case. Now, the only non-zero stream-function component becomes $\partial_3 \Psi_2 = -A_0 x_3$. The only non-zero component of the dimensionality tensor equals $D_{33} = (A_0 x_3)^2$ which is directed in the same direction as the shear (x_3). The only non-zero circulicity component is $F_{22} = (A_0 x_3)^2$ which is directed perpendicular to the streamwise (x_1) and shear directions. As in the former case, all the components of the inhomogeneity tensor are zero.

3 DATA

The data is taken from a direct numerical simulation by Werne and Fritts [22], [23], [6], [24], [16]. The simulation treats the non-linear time evolution of the Kelvin-Helmholtz instability and subsequent turbulent dynamics. It starts with a horizontal laminar shear flow with the hyperbolic-tangent velocity profile $u_1 = U_0 \tanh(z/h)$ and a temperature field represented by a constant vertical temperature gradient $\partial_z T$. U_0 is half the velocity difference across the shear layer, and h is half of the initial shear-layer depth. The minimum initial Richardson number Ri occurs at midlayer ($z = 0$) and is given by $Ri = g\alpha\partial_z T / (\partial_z U)^2 = 0.05$. Here g and α are the acceleration due to gravity and the thermal expansion coefficient, respectively. Early in the simulation, the flow is relatively laminar and two dimensional. As time progresses, turbulence results and the flow becomes three-dimensional. In the later part of the simulation, the turbulence decays and the fluid restratifies into more or less horizontal layers. All dynamical scales are well resolved at all times. The solutions are represented by Fourier modes in the two horizontal directions and sine/cosine series in the vertical direction. When the intensity of the turbulence is at its maximum, the Reynolds-number is $Re = U_0 h / \nu = 2500$, and $1200 \times 400 \times 2400$ modes are used to resolve each field. ν is the kinematic viscosity of the fluid. As the flow evolves, the layer grows to a depth of $L \approx 6h$, so that the layer Reynolds number becomes $Re_L = 2U_0 L / \nu \approx 30,000$.

4 VISUALIZATION

To visualize the energy-containing turbulence structures we apply the structure-based single-point turbulence model and render the structure-based tensors using volume-visualization techniques. This sets the stage for a more complete picture of the properties of turbulent flows. In order to properly study features in volume data sets, the ability to perform interactive visualizations of the volumetric data is necessary. This includes manipulation of transfer functions, clip planes, data-subset selections, and other user functions at interactive rates. We use texture-based direct rendering [2], [5] which allows the necessary interactivity.

The structure-based tensor data are visualized through the largest eigenvalues and the corresponding eigenvectors. The eigenvectors are visualized using the Seed LIC method proposed by Helgeland and Andreassen [8], [9]. The Seed LIC method, which is a method for computing 3D LIC textures, is based on the two techniques proposed by Stalling and Hege [18] and Interrante and Grosch [11]. The technique exploits the sparsity of the input textures by calculating field lines and computing the convolution starting from a set of distributed points (seed points) only. Seed LIC is therefore well suited for visualizing large three-dimensional vector fields. The seed points are randomly distributed inside a Region Of Interest (ROI), using a minimum distance between the seed points to prevent the field lines from residing too close to each other. Since the dynamics of the turbulence flow field is governed by the energy-containing structures, we use kinetic energy to define the ROI in all the Seed LIC computations in this paper.

To study multiple fields at the same time we employ two-field visualization techniques using texture-based direct rendering. This is either done by using two independent sets of color and opacity tables (as shown in Figures 1, 9 and 10) or by letting one of the fields define the structure or “body” through opacity and the other field define the color. Two examples of the last method are shown in Figure 4 and 5. In both examples, the kinetic energy is used to define the opacity while the Seed LIC textures (revealing the eigenvector field of the dimensionality and circulicity tensors) are used to define the color. The latter two-field visualization technique is an excellent method for visualizing directional information of a three-dimensional vector field inside a ROI defined by a scalar

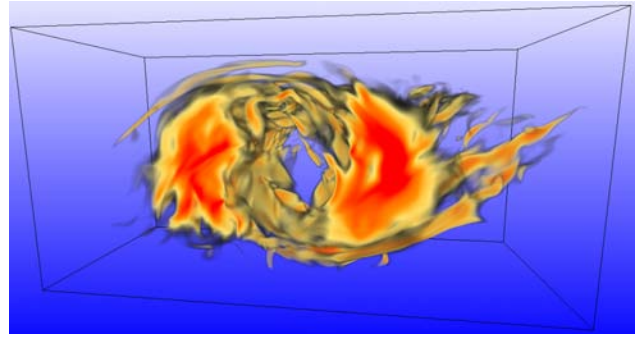


Figure 3: Visualization of the largest eigenvalue of the dimensionality tensor D_{ij} ($t = 105 h/U_0$).

field and was first presented by Helgeland and Andreassen [8], [9]. The technique is especially useful when used in conjunction with interactive clip planes, enabling the user to follow field lines from a 3D LIC texture inside volume data features such as structures in a turbulent flow.

All of the images in this paper were created with Viz [21] and VoluViz [7]; both 3D volume-rendering tools were developed at NDRE (Norwegian Defence Research Establishment).

5 RESULTS AND DISCUSSION

Traditionally, statistical measures are used to handle the enormous amount of data generated by DNS, whereby a lot of detailed information is inevitably lost. Here we perform a point-wise rendering of the structure-based tensors to look into their spatial distribution and “hot spot” regions.

In Figure 1 and Figures 3-6, corresponding to time $t = 105 h/U_0$ in the simulation, various quantities are shown at an early phase of the evolution of the Kelvin Helmholtz billow. Figure 1 shows the regions where λ_2 , the second eigenvalue of the squared rate of strain and rotation tensors $\mathbf{S}^2 + \mathbf{\Omega}^2$, have negative values. This is where the vortex cores are located. In order to show the differences between dissipative (small-) and energetic (large-) scale turbulence, the kinetic energy is also rendered in the same scene.

According to equation (9), the spectrum of the components of D_{ij} , F_{ij} and C_{ij} and their eigenvalues are comparable to that of the turbulent kinetic energy (the first two are symmetric tensors with real eigenvalues and orthogonal eigenvectors). The consequence is that visualization of these tensors will reveal structural information about turbulence mostly at the energy containing scales. This is distinctly different from the information carried by methods based on the velocity derivatives, such as λ_2 .

The eigenvalues of the dimensionality tensor D_{ij} are denoted by σ_1, σ_2 and σ_3 , where $\sigma_1 \geq \sigma_2 \geq \sigma_3 \geq 0$. The rendering of σ_1 is shown in Figure 3; notice the similarity with kinetic energy. In Figure 4, field lines of the eigenvector field corresponding to σ_1 are shown. These field lines are oriented in the direction where the variation of the velocity field is the largest. At time $t = 105 h/U_0$, which is early in the evolution, the core of the Kelvin Helmholtz billow rotates nearly like a solid body. Farther out from the center there is differential rotation. This causes σ_1 to dominate over the other eigenvalues and the corresponding eigenvectors are directed mostly in the radial direction as shown in Figure 4. The circulicity eigenvectors that correspond to the largest eigenvalues ϕ_1 of the circulicity tensor F_{ij} are basically directed along the rotation axis of the Kelvin Helmholtz billow (see Figure 5). In contrast to λ_2 , which depicts the small-scale turbulence, the rendering of the circulicity tensor describes the large-scale structure of the vorticity

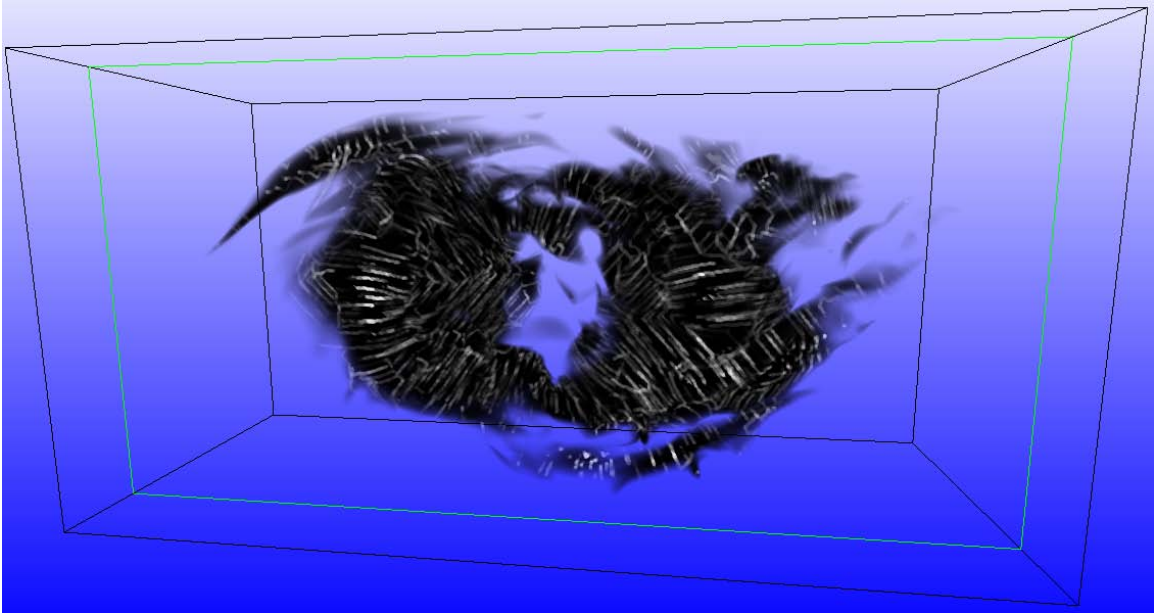


Figure 4: Two-field visualization of the eigenvectors corresponding to the largest eigenvalues of the dimensionality tensor and kinetic energy at time $t = 105 h/U_0$. The kinetic energy is used to define the opacity while the eigenvector field represented by a Seed LIC texture is used to define the color.

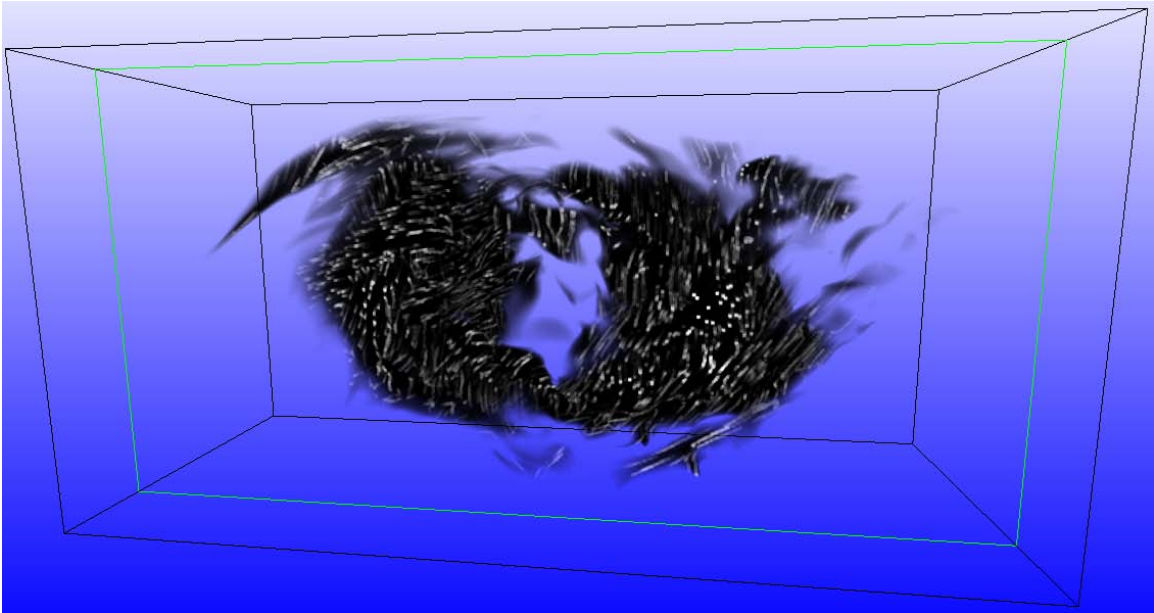


Figure 5: Two-field visualization of the eigenvectors corresponding to the largest eigenvalues of the circulicity tensor and kinetic energy at time $t = 105 h/U_0$. The kinetic energy is used to define the opacity while the eigenvector field represented by a Seed LIC texture is used to define the color.

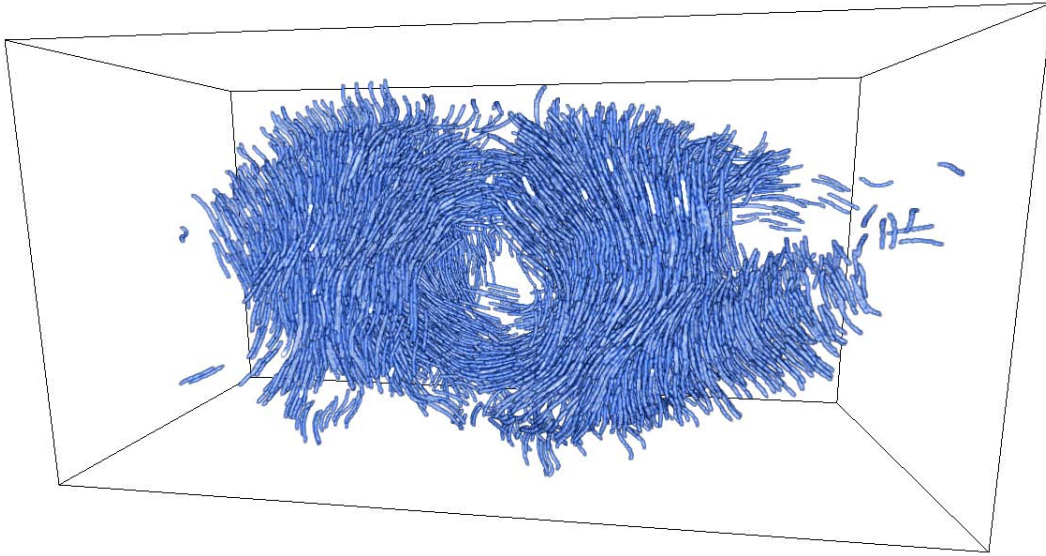


Figure 6: Visualization of the fluctuating velocity field using Seed LIC ($t = 105 h/U_0$).

field, corresponding well with the fluctuating velocity field seen in Figure 6. The rotating motion shown in this image is not revealed by visualizing for example λ_2 , as shown in Figure 1.

The results above are very much as one would expect. The direction of the largest eigenvector of the dimensionality tensor is almost radial, while the eigenvectors corresponding to the largest eigenvalues of the circulicity tensor are mostly oriented along the rotation axis of the billow. The renderings show a great similarity between kinetic energy, σ_1 and ϕ_1 (which is rendered in Figure 7).

At time $t = 270 h/U_0$, the fluid starts to re-stratify (by comparison, the turbulence intensity is maximal near $t \approx 160 h/U_0$). There are still local vortices present, but the kinetic energy appears in elongated and flat structures as seen in Figure 8. Contrary to the early stages of the simulation, the eigenvectors corresponding to the largest eigenvalues of the dimensionality and circulicity tensors have changed direction. The eigenvectors corresponding to the largest eigenvalues of the dimensionality tensor are mostly oriented perpendicular to the flat structures as shown in Figure 9. The corresponding circulicity eigenvectors are oriented more in the vertical plane (x, z) (see Figure 10). This indicates more rotation with a rotational axis oriented in the vertical plane. Both of these features arise from the effectiveness of confinement by stratification at late times. The less vigorous turbulence at $t = 270 h/U_0$ can no longer overcome gravity's restoring force, and overturning motion in the vertical is strongly impeded. This gives rise to motions organized predominantly in horizontal planes.

6 CONCLUDING REMARKS

A novel approach for visualizing the energetic structures of a turbulent flow field using single-point structure-based tensors together with volume rendering has been assessed. To this end, the flow field resulting from the nonlinear evolution of a Kelvin-Helmholtz instability in a stratified environment has been investigated. For the first time, volume visualization has been used in conjunction with structure-based tensors. These tensors, combined with the Reynolds-stress tensor, form a minimal tensorial base for a complete one-point turbulence theory. Structure-based tensors yield additional information about the energetic turbulent structures that is different from the information carried by the fluctuating velocity components themselves. The information is also distinctly differ-

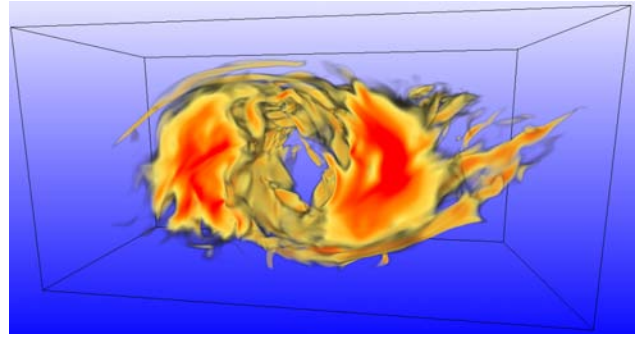


Figure 7: Visualization of the largest eigenvalue of the circulicity tensor F_{ij} ($t = 105 h/U_0$).

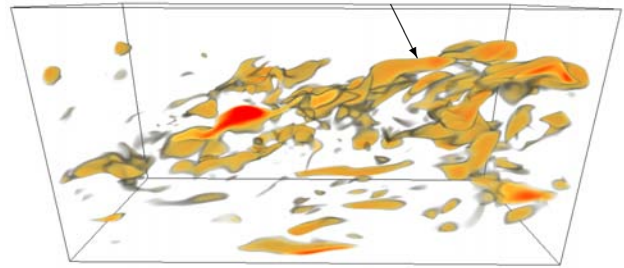


Figure 8: Visualization of kinetic energy ($t = 270 h/U_0$).

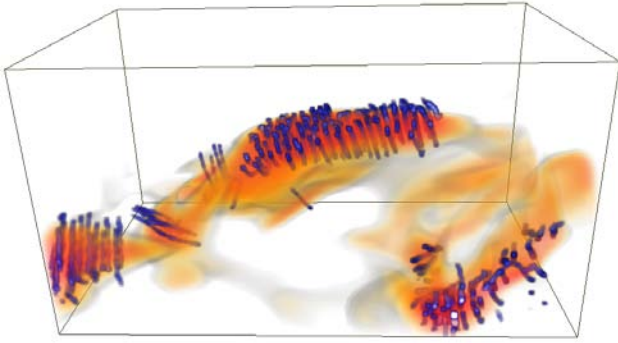


Figure 9: Two-field visualization of kinetic energy and the eigenvectors corresponding to the largest eigenvalues of the dimensionality tensor at time $t = 270 h/U_0$. The Figure shows a small subset of the full domain revealing only a few structures in the area indicated by the arrow in Figure 8.

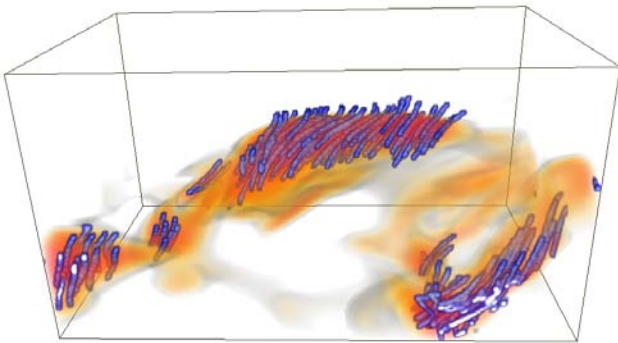


Figure 10: Two-field visualization of kinetic energy and the eigenvectors corresponding to the largest eigenvalues of the circulicity tensor at time $t = 270 h/U_0$. The Figure shows a small subset of the full domain revealing only a few structures in the area indicated by the arrow in Figure 8.

ent from the small-scale features represented by traditional techniques such as λ_2 as demonstrated in this paper. The outcome of this study is that point-wise volume visualization used in conjunction with structure-based tensors constitutes a new and promising tool in turbulence research.

7 ACKNOWLEDGMENTS

We would like to thank Dr. Dave Fritts (NorthWest Research Associates, Colorado Research Associates Division) for valuable discussions.

REFERENCES

[1] D. C. Banks and B. A. Singer. A Predictor-Corrector Technique for Visualizing Unsteady Flow. *IEEE Transactions on Visualization and Computer Graphics*, 1(2):151–163, June 1995.

[2] B. Cabral, N. Cam, and J. Foran. Accelerated Volume Rendering and Tomographic Reconstruction Using Texture Mapping Hardware. In *Proceedings 1994 Symposium on Volume Visualization*, pages 91–98, October 1994.

[3] M. S. Chong, A. E. Perry, and B. J. Cantwell. A general classification of three-dimensional flow fields. *Phys. Fluids*, 2:765–777, 1990.

[4] P. Compte, J. Silvestrini, and P. Begou. Streamwise vortices in large eddy simulation of mixing layers. *Eur. J. Mech. B*, 17:615–937, 1998.

[5] T. J. Cullip and U. Neumann. Accelerated Volume Reconstruction with 3D Texture Mapping Hardware. Technical Report TR93-027, Department of Computer Science, University of North Carolina, May 1994.

[6] D. C. Fritts and J. Werne. Turbulence Dynamics and Mixing due to Gravity Waves in the Lower and Middle Atmosphere. In *Atmospheric Science across the Stratopause*, number 123 in Geophysical Monograph, pages 143–159. American Geophys. Union, 2000.

[7] T. Gaarder and A. Helgeland. VoluViz 1.0 Report. Technical Report FFI/RAPPORT-2002/03449, FFI (Norwegian Defence Research Establishment), September 2002.

[8] A. Helgeland and O. Andreassen. Interactive Poster: Visualization of Vector Fields Using LIC and Volume Rendering. In *IEEE Visualization 2002, Poster Compendium*, pages 84–85, October–November 2002.

[9] A. Helgeland and O. Andreassen. Visualization of Vector Fields Using Seed LIC and Volume Rendering. *IEEE Transactions on Visualization and Computer Graphics*, 2004. (In press).

[10] J. C. R. Hunt, A. A. Wray, and P. Moin. Eddies, streams, and convergence zones in turbulent flows. In *Proceedings of the Summer Program 1988*, pages 193–208. Stanford University, Center for Turbulence Research, 1988.

[11] V. Interrante and C. Grosch. Visualizing 3D Flow. *IEEE Computer Graphics and Applications*, 18(4):49–53, July–August 1998.

[12] J. Jeong and F. Hussain. On the identification of a vortex. *J. Fluid Mech.*, 285:765–777, 1995.

[13] M. Jiang, R. Machiraju, and D. S. Thompson. A Novel Approach To Vortex Core Region Detection. In *Joint Eurographics - IEEE TCVG Symposium on Visualization*, pages 217–225, may 2002.

[14] S. C. Kassinos, W. C. Reynolds, and M. M. Rogers. One-point turbulence structure tensors. *J. Fluid Mech.*, 428:213–248, 2001.

[15] M. Lesieur. *Turbulence in Fluids*. Dordrecht: Kluwer, 1997.

[16] B. A. P. Reif, J. Werne, Ø. Andreassen, C. Meyer, and M. Davis-Mansour. Entrainment-zone restratification and flow structures in stratified shear turbulence. In *Studying Turbulence Using Numerical Simulation Databases - IX*, Proceedings of the Summer Program 2002, pages 245–256. Center for Turbulence Research, Stanford University, December 2002.

[17] M. Roth and R. Peikert. A Higher-Order Method For Finding Vortex Core Lines. In *Proceedings of Visualization '98*, pages 143–150, October 1998.

[18] D. Stalling and H.-C. Hege. Fast and Resolution Independent Line Integral Convolution. In *Computer Graphics Proceedings, Annual Conference Series*, pages 249–256, August 1995.

[19] D. Sujudi and R. Haimes. Identification of Swirling Flow in 3D Vector Fields. In *Proceedings of the 12th AIAA Computational Fluid Dynamics*, pages 792–799, jun 1995.

[20] H. Tennekes and J. L. Lumley. *A First Course in Turbulence*. MIT Press, 1972.

[21] Viz. Information and software. Available on the web at the URL, <ftp://ftp.ffi.no/pub/stsk/viz/features.html>.

[22] J. Werne and D. C. Fritts. Stratified shear turbulence: Evolution and statistics. *Geophys. Res. Letters*, 26:439–442, 1999.

[23] J. Werne and D. C. Fritts. Anisotropy in a stratified shear layer. *Physics and Chemistry of the Earth*, 26:263, 2000.

[24] J. Werne and D. C. Fritts. Structure Functions in Stratified Shear Turbulence. In *DoD HPC User Group Conference*. Albuquerque, NM, 2000.